

## Supplemental Information for

### **A Ciprofloxacin Derivative with Four Mechanisms of Action Overcomes Paclitaxel Resistance in p53-Mutant and MDR1 Gene-Expressing Type II Human Endometrial Cancer**

Suhaila O. Alhaj-Suliman, Youssef W. Naguib, Emad I. Wafa, Sanjib Saha, Kareem Ebeid, Xiangbing Meng, Hamada H. Mohammed, Gamal El-Din A. Abuo-Rahma, Shujie Yang, Aliasger K. Salem\*

\* Correspondence to: [aliasger-salem@uiowa.edu](mailto:aliasger-salem@uiowa.edu)

#### **This file includes:**

Supplementary Tables

Supplementary Figures

## Supplementary Tables

**Table S1.** Estimated IC<sub>50</sub> values (expressed as nM of either PTX or DOC) for indicated cell line following treatment with either PTX ± CIP2b or DOC ± CIP2b.

	<b>Ishikawa-H WTp53</b>	<b>Hec50co LOFp53</b>	<b>Hec50co GOFp53</b>	<b>KLE GOFp53</b>
PTX	2.593 ± 0.134	5.137 ± 0.303	3.593 ± 0.165	5.424 ± 0.363
PTX + 1 μM CIP2b	2.534 ± 0.137	4.148 ± 0.132	2.581 ± 0.130	5.195 ± 0.478
PTX + 10 μM CIP2b	2.250 ± 0.152	1.693 ± 0.291	1.969 ± 0.099	3.139 ± 0.338
PTX + 20 μM CIP2b	1.765 ± 0.103	1.456 ± 0.426	1.481 ± 0.383	1.439 ± 0.529
PTX + 10 μM CIP	2.790 ± 0.180	6.096 ± 0.352	3.757 ± 0.213	4.844 ± 0.438
DOC	0.319 ± 0.013	1.381 ± 0.062	0.837 ± 0.053	5.11 ± 0.451
DOC + 1 μM CIP2b	0.226 ± 0.023	0.564 ± 0.156	0.319 ± 0.172	2.673 ± 0.165
DOC + 10 μM CIP2b	0.095 ± 0.021	0.687 ± 0.100	0.176 ± 0.067	2.204 ± 0.131
DOC + 20 μM CIP2b	0.040 ± 0.048	0.628 ± 0.053	0.039 ± 0.033	1.409 ± 0.238
DOC + 10 μM CIP	0.250 ± 0.026	1.377 ± 0.043	2.008 ± 0.058	4.844 ± 0.438

**Table S2.** Selected grid box parameters for protein targets (human MDR1,  $\alpha\beta$ -tubulin, Topo I, and Topo II).

<b>Target</b>	<b>Centre Grid Box (Å in X, Y, Z-axis)</b>	<b>Size (Å in X, Y, Z-axis)</b>
MDR1	173.33 × 166.742 × 161.482	25 × 25 × 25
Topo I	21.473 × -2.226 × 27.863	20 × 20 × 20
Topo II (1 <sup>st</sup> binding site of ETO)	31.341 × -23.166 × -57.75	25 × 25 × 25
Topo II (2 <sup>nd</sup> binding site of ETO)	23.307 × -38.584 × -59.568	25 × 25 × 25
$\alpha\beta$ -tubulin	0.702 × -16.806 × 14.694	25 × 25 × 25

**Table S3.** Binding energies and interacting residues for protein targets (human MDR1,  $\alpha\beta$ -tubulin, Topo I, and Topo II).

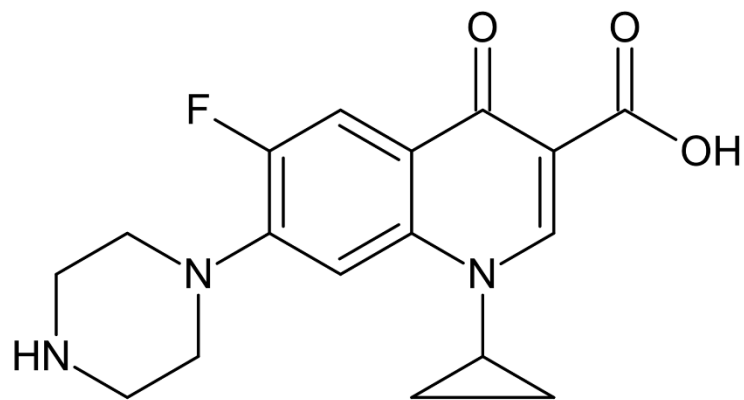
<b>Targets</b>	<b>Target binding pocket</b>	<b>Lowest binding energy (kcal/mol)</b>	<b>Interacting residues</b>	<b>Residues forming H-bonds</b>
MDR1	PTX	-10.8	LEU65, GLN195, THR199, PHE303, TYR307, ILE340, PHE343, SER344, LEU724, GLN725, SER766, ASN842, GLN946, MET949, MET986, ALA987, GLN990	SER344
Topo I	CAM	-10.8	DG12, DA13, DC112, DA 113, DT10, ALA351, ASN 352, ARG364, TYR426, ILE427, MET428, LEU429, LYS436	DG12, DC112, ARG364, MET428
Topo II	ETO (1 <sup>st</sup> site)	-12.0	DC8, DT9, DA12, DG13, GLY462, ARG487, GLY488, ASP541, HIS759, GLY760, MET762, SER763, MET766, TYR805	DC8, DA12
Topo II	ETO (2 <sup>nd</sup> site)	-12.9	DC8, DT9, DA12, DG13, GLY462, ARG487, GLY488, ALA505, GLU506, ASP541, GLY760, MET762, SER763, HIS759, TYR805	DC8, ARG487
$\alpha\beta$ -tubulin	PTX	-9.6	VAL23, GLU27, LEU217, LYS218, LEU219, HIS229, ALA233, SER236, GLY237, PHE272, SER277, ARG278, ARG320, PRO360	LEU219

**Table S4.** Band intensity of the Western blot analysis to evaluate the effect of PTX ± CIP2b on cell cycle regulatory proteins in Hec50co LOFp53 cells. Data are reported as relative percentages to the band intensity of the untreated cell samples.

	<b>cdc2</b>	<b>Phospho-cdc2-Tyr15</b>	<b>Cdc25C</b>
PTX 40 nM	87.93%	21.02%	29.98%
PTX 40 nM + 10 μM CIP2b	76.62%	2.15%	9.49%
PTX 40 nM + 25 μM CIP2b	69.39%	0.93%	5.41%
PTX 40 nM + 50 μM CIP2b	66.79%	2.28%	10.84%
CIP2b 10 μM	68.00%	57.18%	99.09%
CIP2b 25 μM	80.40%	63.51%	98.05%
CIP2b 50 μM	69.50%	48.06%	96.41%

## Supplementary Figures

**a**



**b**

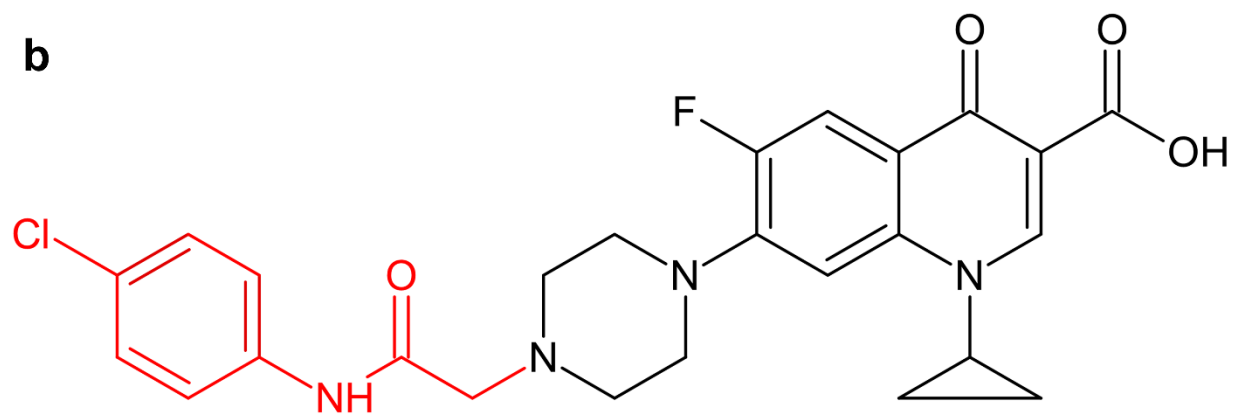


**Fig. S1.** Chemical structures of (1) ciprofloxacin (CIP) and (b) its derivative (CIP2b).

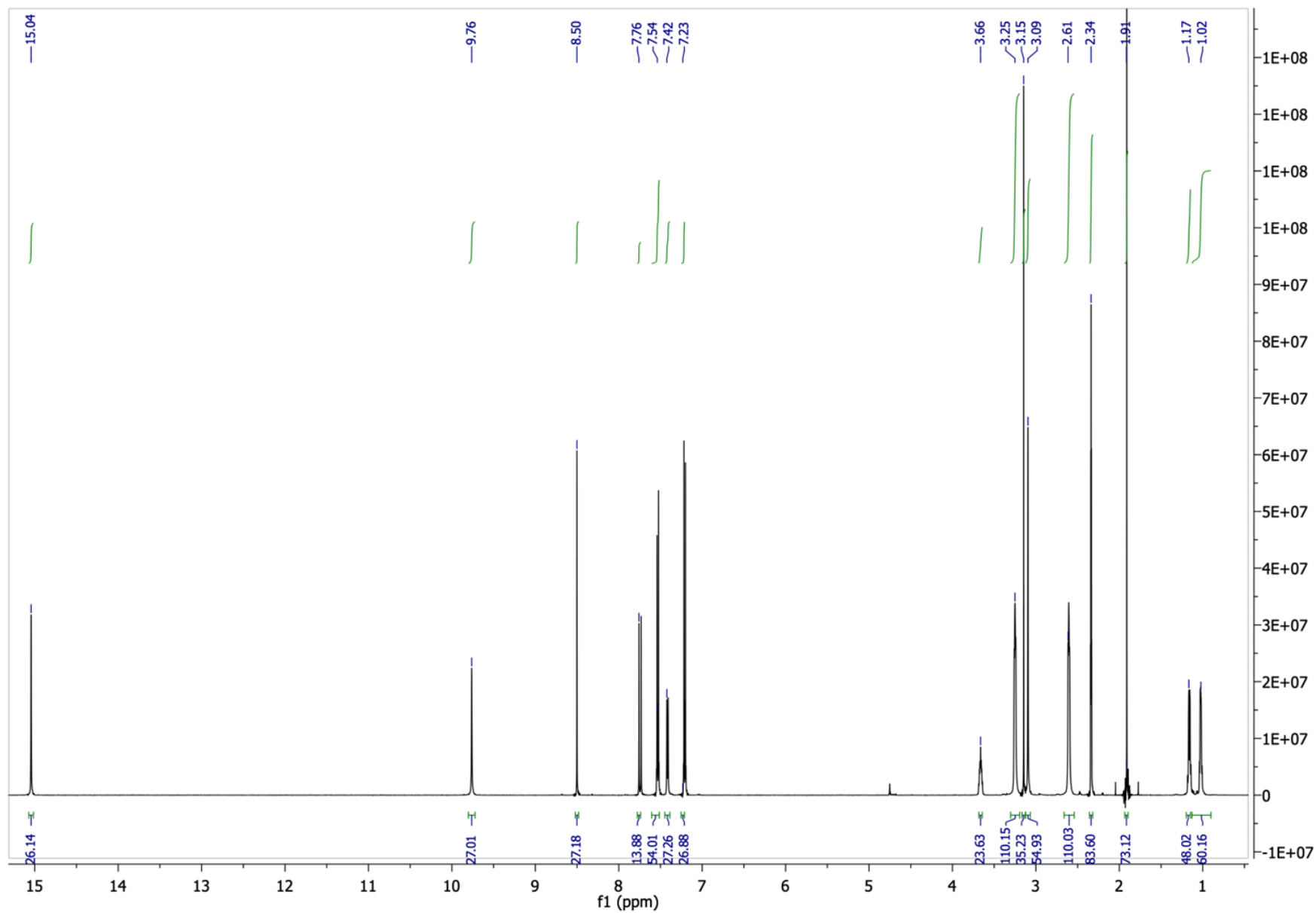
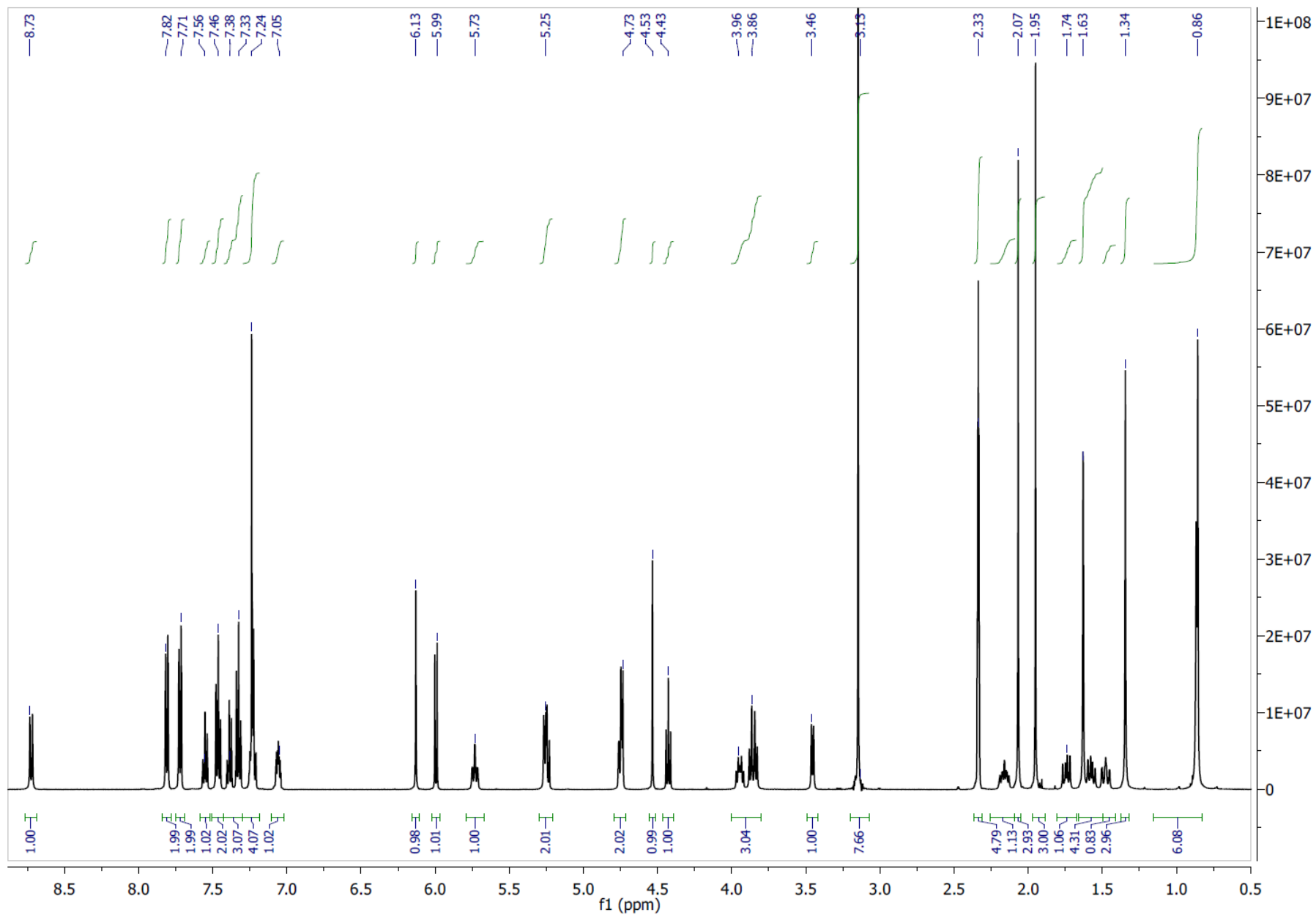
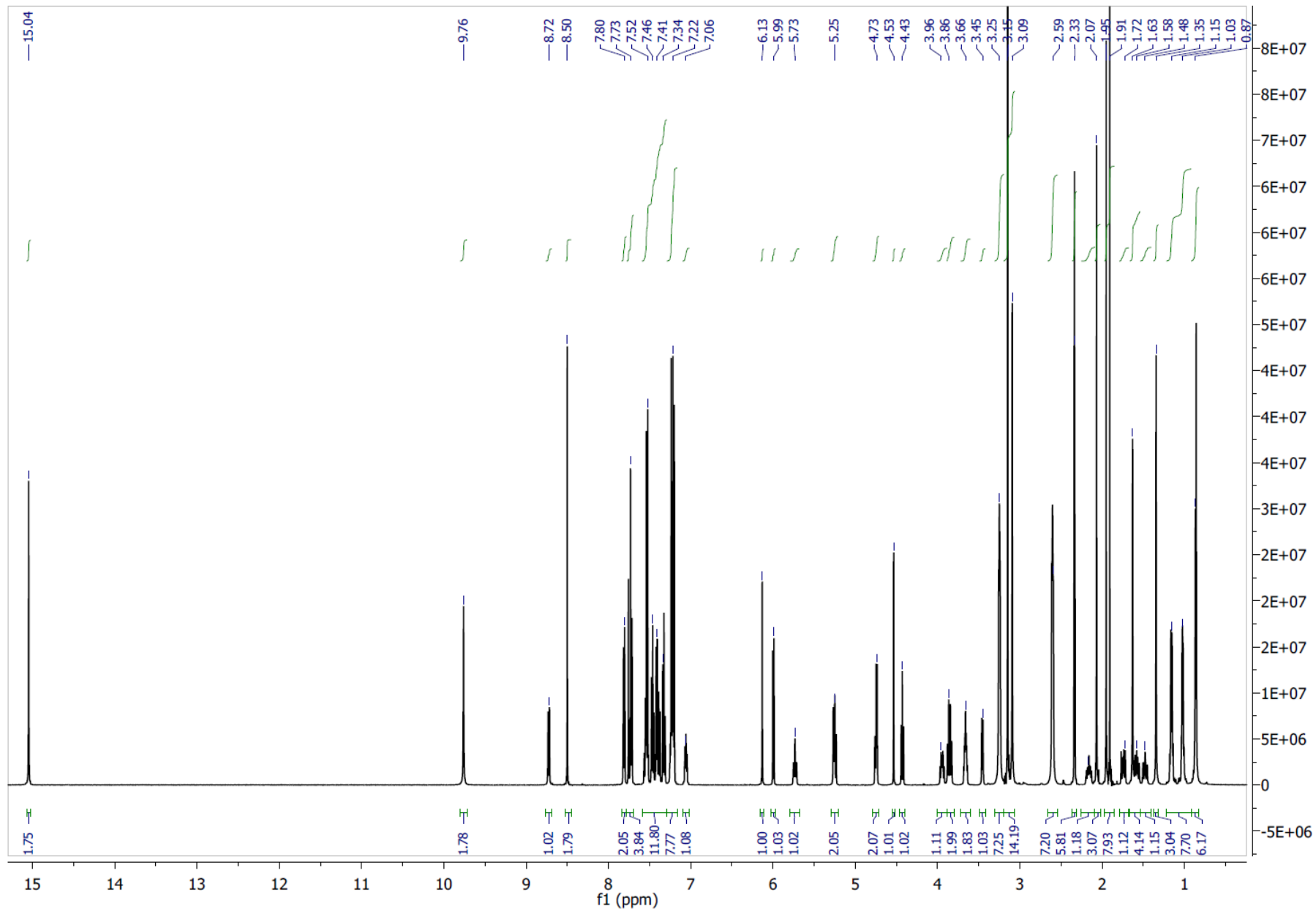


Fig. S2. <sup>1</sup>H NMR spectrum of CIP2b.



**Fig. S3.** <sup>1</sup>H NMR spectrum of PTX.



**Fig. S4.**  $^1\text{H}$  NMR spectrum of PTX + CIP2b.

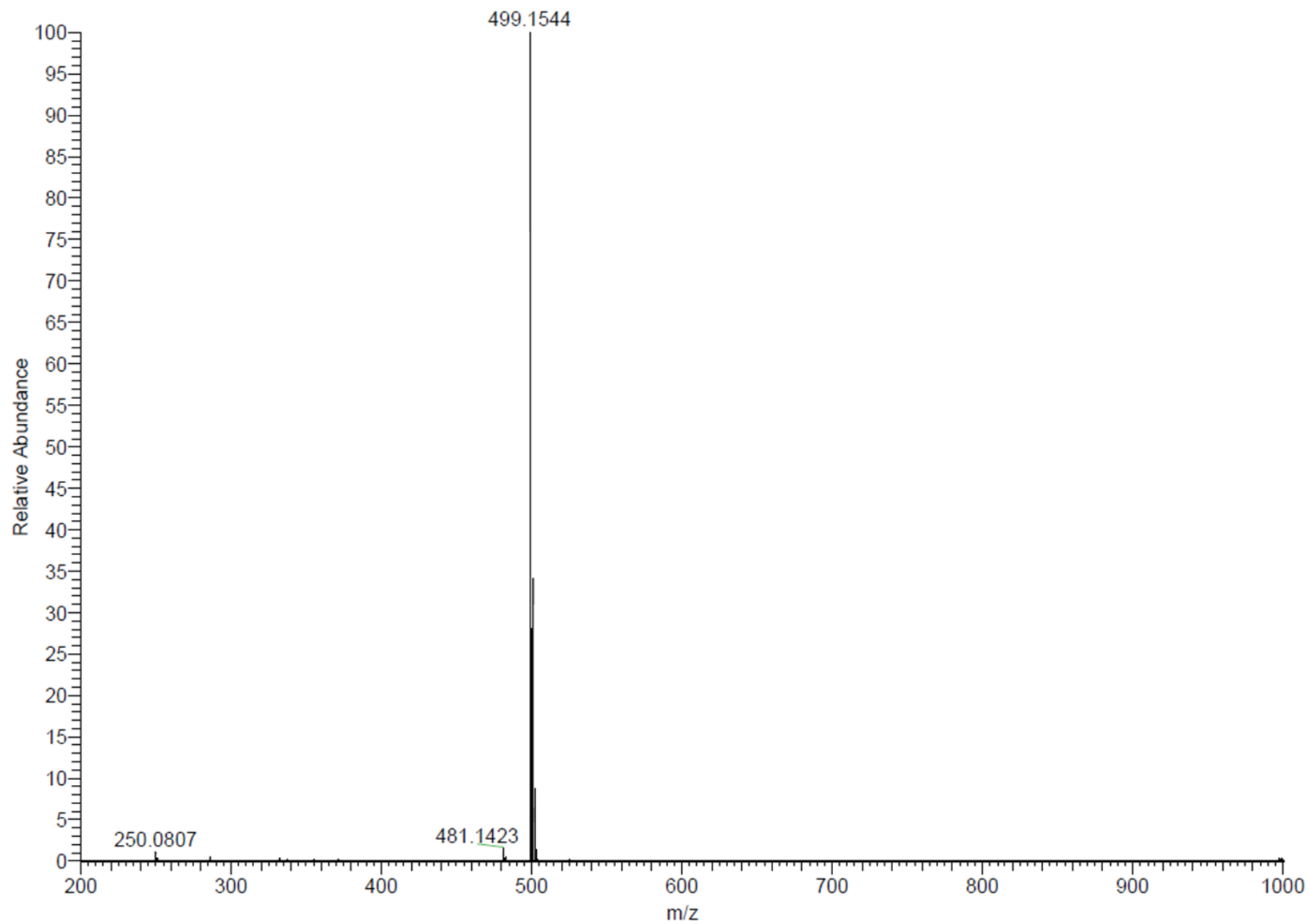


**Fig. S5.** Electrospray ionization mass spectrometry analysis of CIP2b.

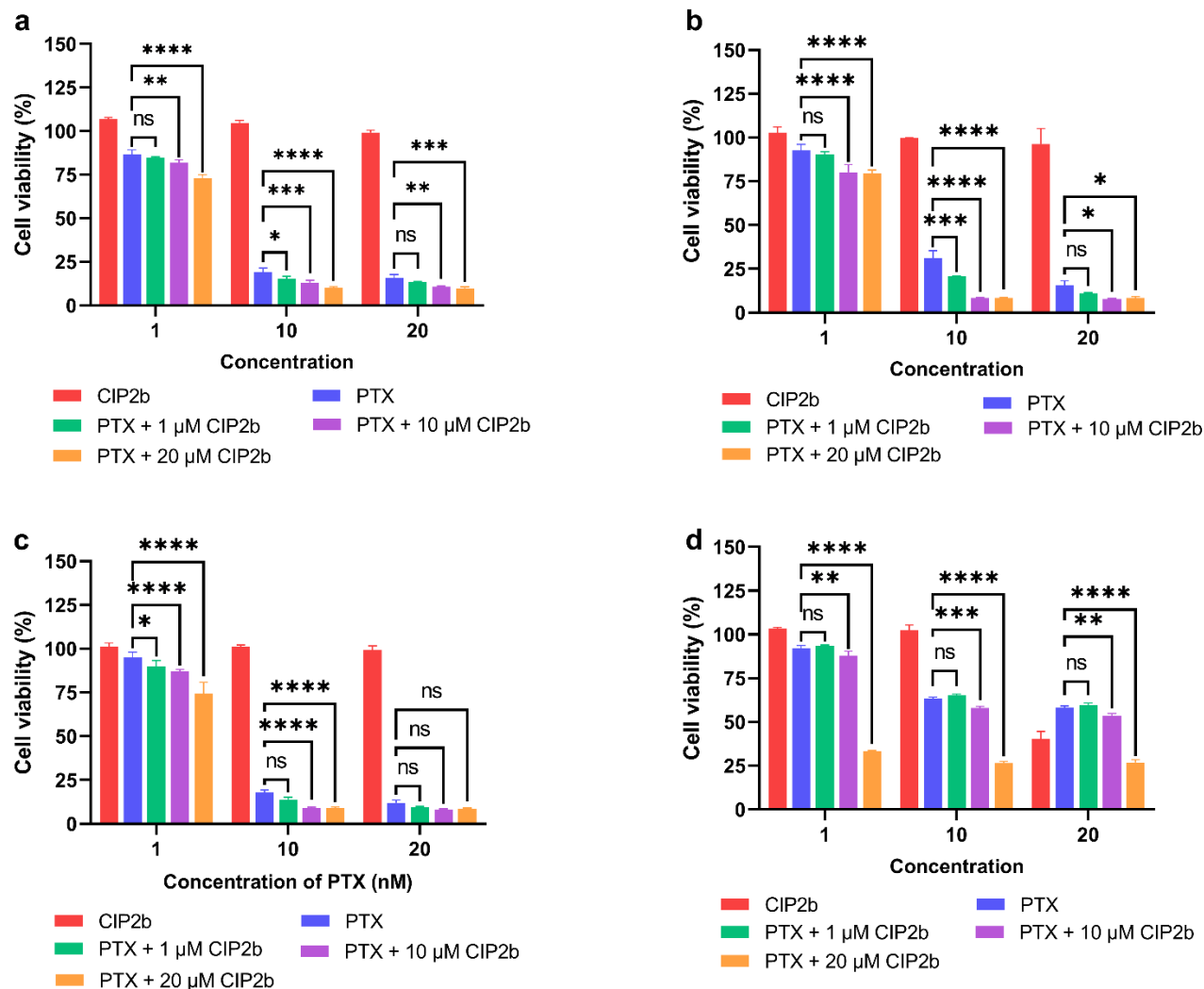


**Fig. S6.** *In vitro* antitumor effect of the PTX + CIP2b drug combination against different endometrial cancer cell lines. (a–d) Survival analysis of Ishikawa-H WTp53, Hec50co LOFp53, Hec50co GOFp53, and KLE GOFp53 cells, respectively, treated for 72 hours with different concentrations of PTX (1, 10, and 20 nM) and CIP2b (1, 10, and 20  $\mu$ M). A two-way ANOVA with the Tukey *post hoc* test was used for statistical analysis. Data are plotted as mean  $\pm$  SD (n=3). \*,  $P < 0.05$ ; \*\*,  $P < 0.01$ ; \*\*\*,  $P < 0.001$ ; \*\*\*\*,  $P < 0.0001$ ; ns, nonsignificant.

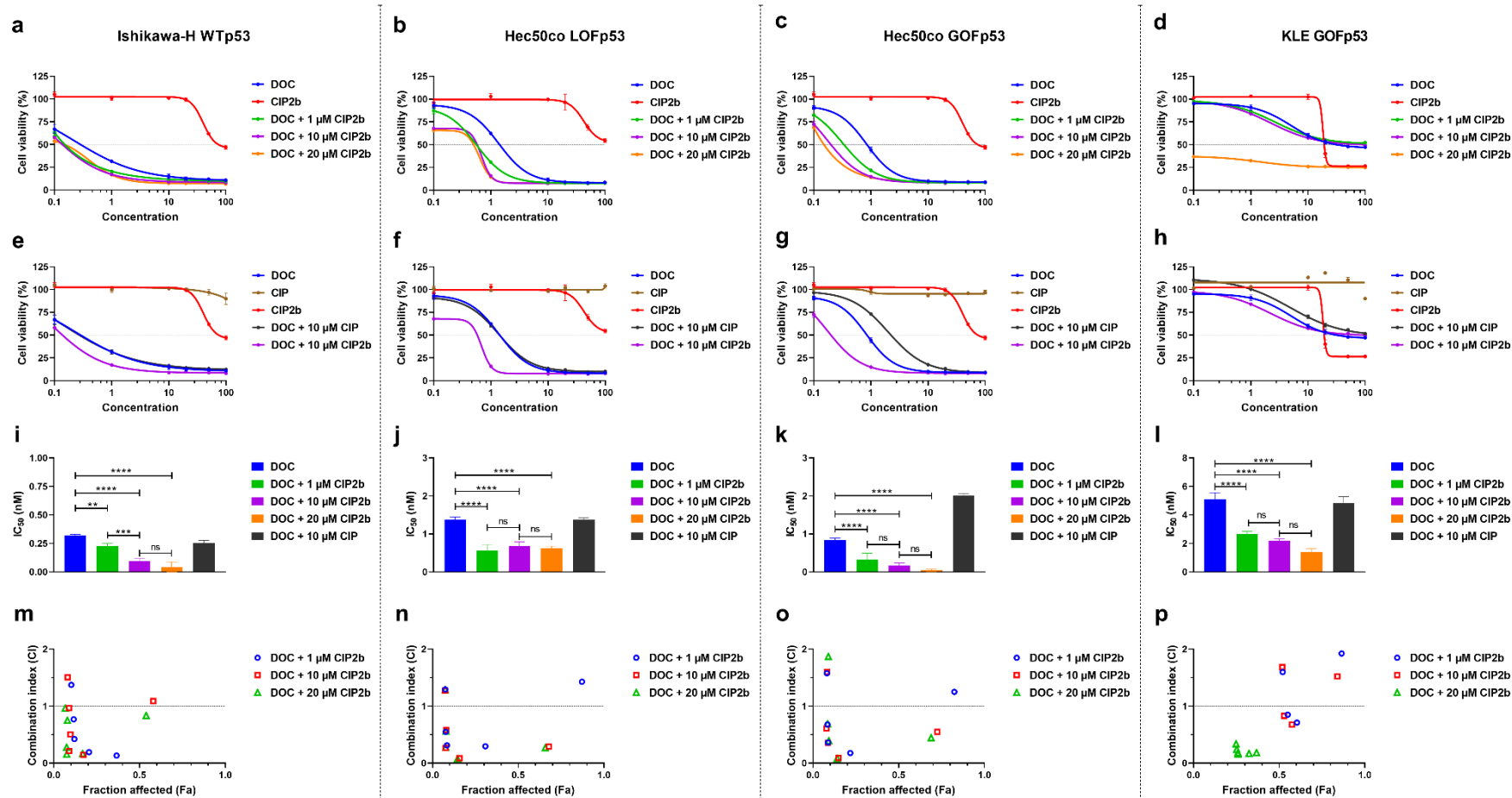


**Fig. S7.** *In vitro* antitumor activity of DOC ± CIP2b combinatorial treatment against four different human endometrial cancer cell lines. (a–d) Cytotoxicity assay for indicated cell line following treatment for 72 hours with different concentrations of either DOC or CIP2b or different concentrations of DOC and fixed concentrations of CIP2b. (e–h) Cytotoxicity assay for indicated cell line following treatment for 72 hours with different concentrations of either DOC or CIP or CIP2b or different concentrations of DOC and fixed concentrations of either CIP or CIP2b. (i–l) Estimated  $IC_{50}$  values for indicated cell line treated with DOC ± CIP or CIP2b. (m–p) Cytotoxic synergy between DOC and CIP2b for the indicated cell line is calculated using the CI method where CI values less than 1 indicate synergy. Data are plotted as mean ± SD ( $n=3$ ). A one-way ANOVA with Tukey *post hoc* test was used for statistical analysis. \*,  $P < 0.05$ ; \*\*,  $P < 0.01$ ; \*\*\*,  $P < 0.001$ ; \*\*\*\*,  $P < 0.0001$ ; ns, nonsignificant.

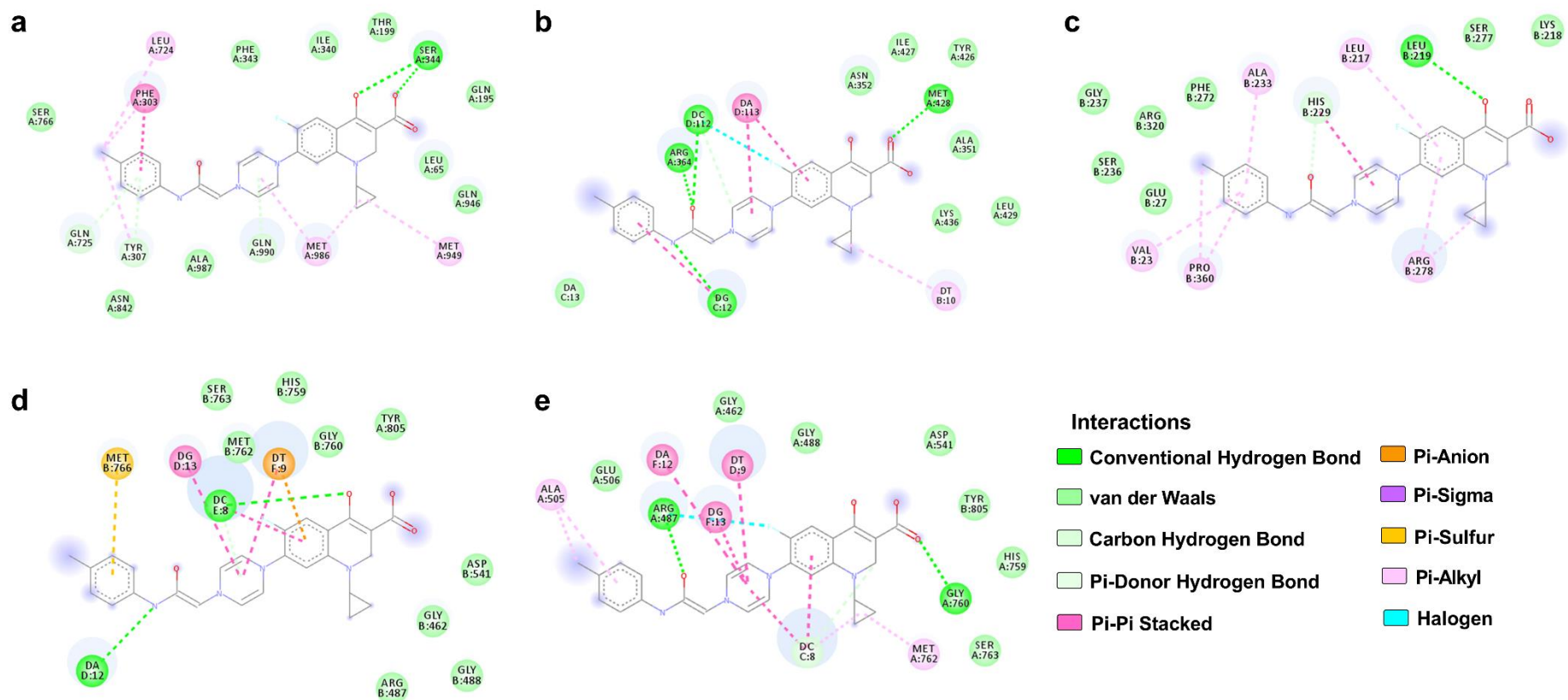


**Fig. S8.** Molecular docking of CIP2b within the binding pockets. 2D diagrams of the molecular docking interactions of CIP2b with different binding sites on human (a) MDR1 in the binding pocket of PTX; (b) Topo I in the binding pocket of CAM; (c) Topo II in the first binding pocket of ETO; (d) Topo II in the second binding pocket of ETO; and (e)  $\alpha\beta$ -tubulin in the binding pocket of PTX.

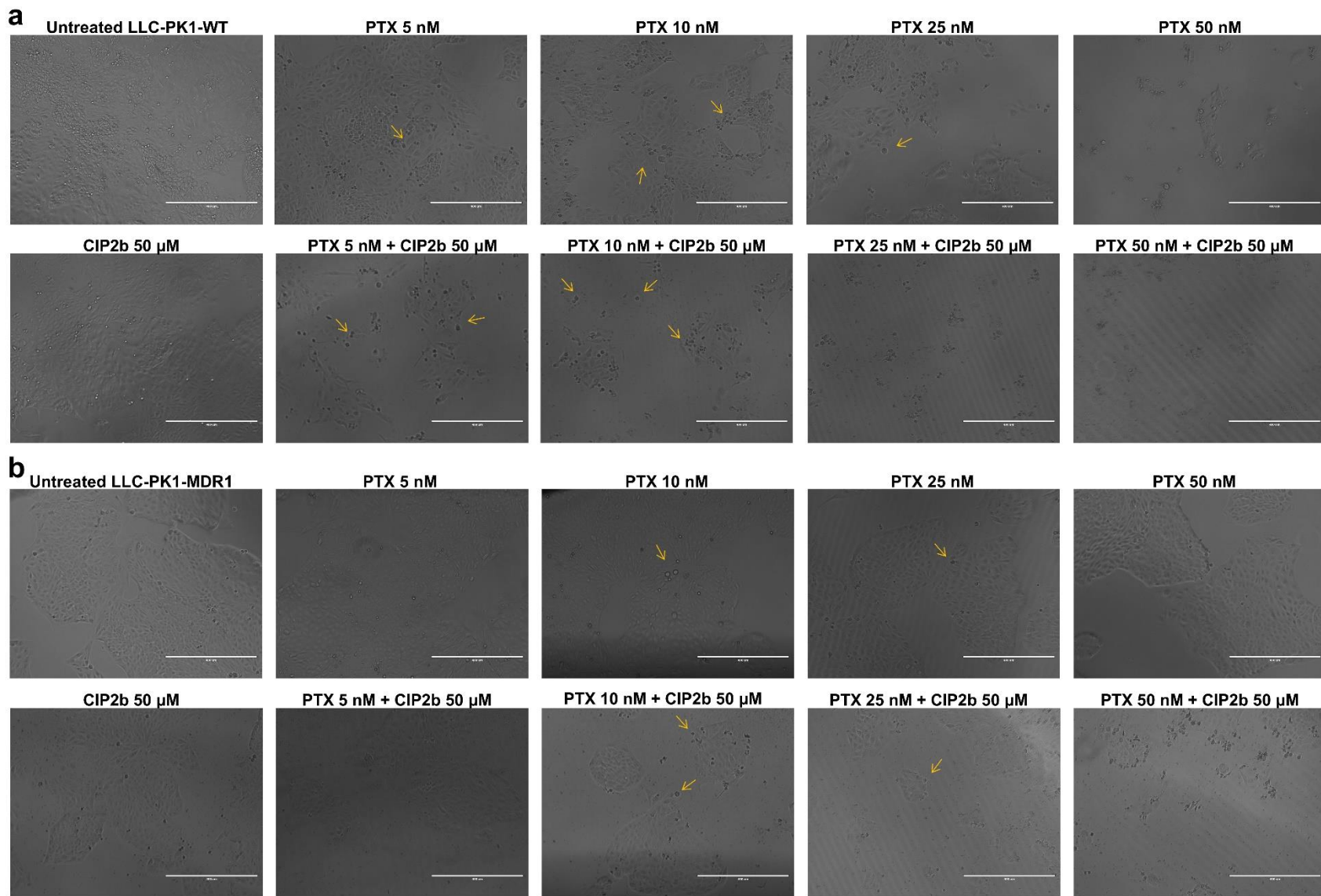


**Fig. S9.** Representative bright-field microscope images of (a) LLC-PK1-WT, and (b) LLC-PK1-MDR1 cells. Cells were untreated or treated for 72 hours with 5 nM PTX in the presence or absence of 50  $\mu$ M CIP2b. Rounded cells represent those undergoing apoptosis (under stress, pointed out by arrows). Images were acquired with a 10x objective lens; the total magnification is 100x. Scale bar = 400  $\mu$ m.

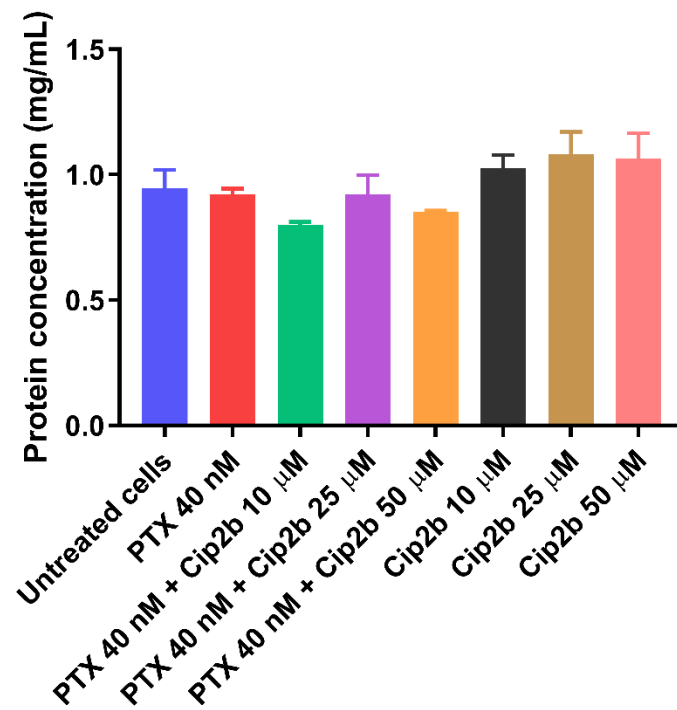


**Fig. S10.** Protein content in the lysate of Hec50co LOFp53 cells incubated with different treatments. Protein concentration was measured using Micro BCA Protein Assay Kit.

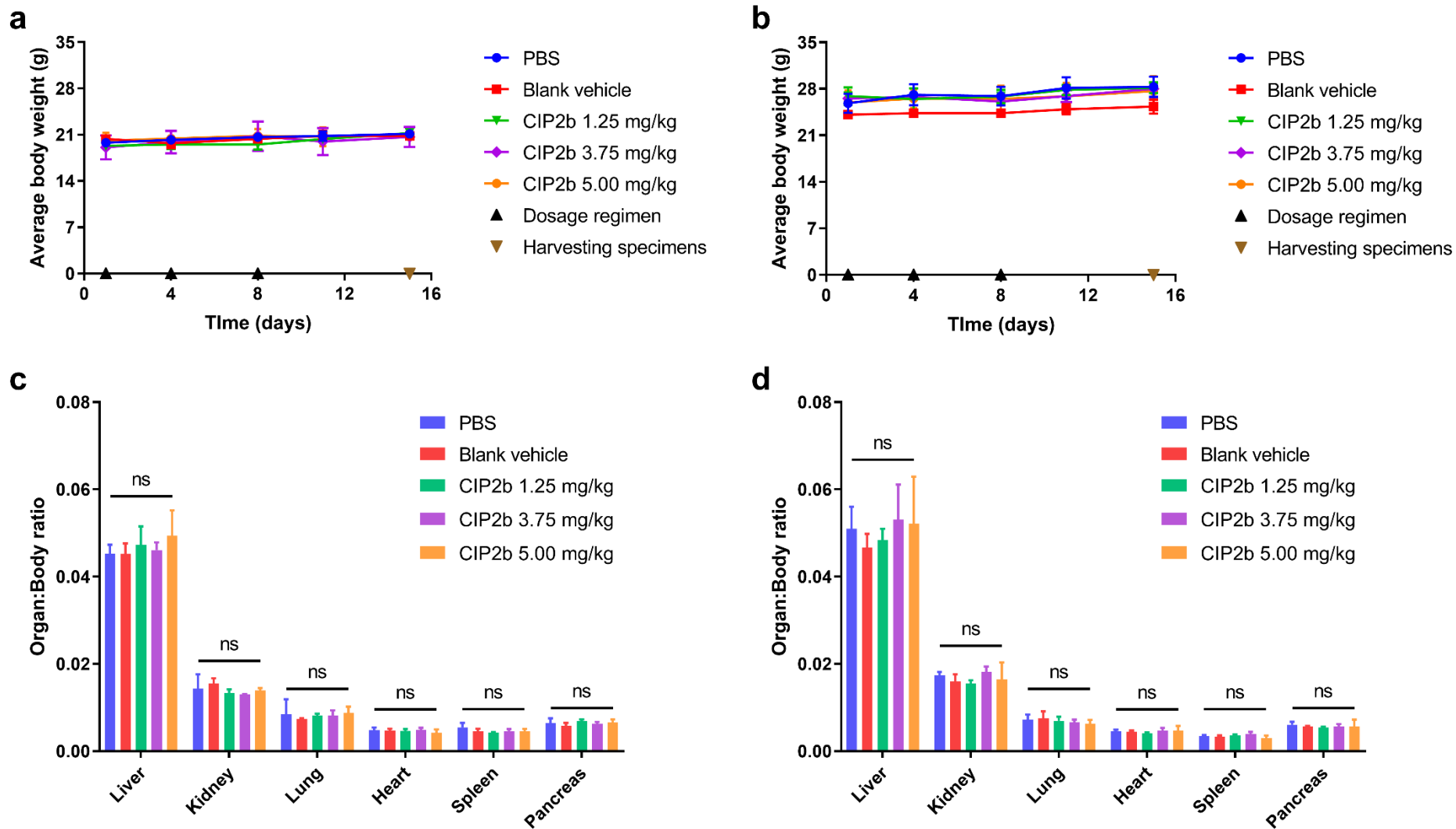


**Fig. S11.** *In vivo* acute toxicity study following IV administration of different doses of CIP2b. (a and b) Body weight monitoring of female and male BALB/c mice, respectively. (c and d) Organ to body weight ratio of female and male BALB/c mice, respectively. Data are plotted as mean  $\pm$  SD (n=3). A two-way ANOVA with the Tukey *post hoc* test was used for statistical analysis. ns, nonsignificant.